ADVANCED INTELLIGENT SYSTEMS
www.advintellsyst.com

Self-Closing and Self-Healing Multi-Material Suction Cups for Energy-Efficient Vacuum Grippers

Zhanwei Wang, Seppe Terryn, Huijiang Wang, Julie Legrand, Ali Safaei, Joost Brancart, Guy Van Assche, and Bram Vanderborght*

While vacuum grippers offer an economical solution, the environmental impact of energy waste through their suction cups (SCs) cannot be overlooked. This waste stems from three key factors: i) air losses from idle SCs arranged in arrays, ii) inadequate sealing on target surfaces leading to air leaks, and iii) damage from sharp objects resulting in leaking perforations. To overcome these challenges, in this article, a comprehensive approach is presented that involves the development of a i) self-closing, ii) multi-material, and iii) self-healing system based on reversible elastomers cross-linked via the Diels–Alder (DA) reaction. The system incorporates a fully autonomous self-closing mechanism to prevent energy waste in SC arrays during periods of non-contact. Fluid–structure interaction simulations are utilized to analyze the design. Versatility and stability are achieved by incorporating hyper-flexible and stiff elastomers in a multi-material design, supported by covalent DA cross-links that ensure robustness through high-strength multi-material interfaces. These DA cross-links also enable self-healing capabilities, allowing the SCs to recover from macroscopic damages within 1 day at ambient conditions or in a single hour with mild heating (80–90 °C), restoring full performance. Additionally, in the article, a recycling method is introduced for multi-material SCs based on the mechanical separation of reversible polymers.

1. Introduction

Vacuum suction cups (SCs) find extensive applications across industries, including assembly and sorting lines, warehouses, packaging, robot movement, and actuation.[1–3] They are utilized as grippers in space[4] and even in medical procedures.[5,6] The popularity of SCs stems from their compactness and high adhesive forces.[7–10] In industrial settings, arrays of SCs are commonly employed to achieve high throughput or enable grippers capable of picking and placing objects of various sizes and shapes.

SCs are divided into active and passive categories. Passive SCs operate based on volumetric change, where the inner air is expelled from the SC upon contact with an object, creating suction force. This approach is energy efficient as it doesn't require external energy consumption.[11,12] However, passive SCs have certain drawbacks. First, controlling the release of passive SCs is challenging. Second, the adhesive force is limited by the maximum volumetric change resulting from shape alteration, making it difficult to predict. Third, leaks cannot be compensated, posing safety risks due to potential increases in pressure (e.g., loss of vacuum) and sudden release. To address this issue, a disc spring-based SC was developed.[13] The spring pulls up the vacuum chamber if there is a leakage. However, this safety measure is limited by the maximum force and deformation of the spring. Additionally, passive SCs require high pre-pressing force to create a seal on surfaces, which can be risky when handling delicate items. In contrast, active SCs rely on external energy to generate adhesive force. In industrial applications, most cups are activated using vacuum generators like rotational vacuum pumps or pistons,[14] controlled by valves such as solenoid or piezo valves. While these systems offer strong adhesion forces and precise attachment and detachment control, they are generally bulky and energy inefficient.

Alternatively, integrating actuation leads to more compact designs in internally activated SCs, eliminating the need for a vacuum generator. This approach utilizes material-based actuation, e.g., stimuli-responsive materials, to actively control the volume change in the SC and generate suction. Motzki et al. developed a shape memory alloy (SMA) driven SC that

Z. Wang, S. Terryn, J. Legrand, B. Vanderborght
Brubotics
Vrije Universiteit Brussel and Imec
Pleinlaan 2, 1050 Elsene, Belgium
E-mail: Zhanwei.wang@vub.be

H. Wang
Department of Engineering
University of Cambridge
Trumpington Street, Cambridge CB2 1PZ, UK

A. Safaei, J. Brancart, G. V. Assche
Physical Chemistry and Polymer Science
Vrije Universiteit Brussel
Pleinlaan 2, 1050 Elsene, Belgium

The ORCID identification number(s) for the author(s) of this article can be found under https://doi.org/10.1002/aisy.202300135.

© 2023 The Authors. Advanced Intelligent Systems published by Wiley-VCH GmbH. This is an open access article under the terms of the Creative Commons Attribution License, which permits use, distribution and reproduction in any medium, provided the original work is properly cited.

DOI: 10.1002/aisy.202300135

achieves a 20 Newton holding force with just 4.5 V.[15] Welsch et al. created a bistable SC using SMA wires, combined with a bistable spring and integrated condition monitoring through the self-sensing effect of SMA.[16] However, the slow recovery of SMA during cooling affects the time efficiency of SMA-actuated SCs, limiting their applications.[17] Lyu et al. proposed a flexible vacuum gripper based on the reversible flat-to-conical deformation of azimuthally aligned liquid-crystal elastomer films, which achieves highly integrated performance, exerting a force that is 100 times its own weight.[18] Nonetheless, this type of material-based actuation also exhibits a slow response. Zhang et al. aimed for low noise generation and energy consumption by developing an SC based on magnetorheological elastomers, weighing 268 g and exerting 8 N suction force.[19] While these examples eliminate the need for an external vacuum generator, the integrated actuation module adds bulk to the end effector. Furthermore, pursuing energy efficiency and compactness often impacts the traditional advantages of externally activated SCs, such as fast response and high adhesion forces. Another drawback of integrated actuation is the increased system complexity when arranging SCs in arrays, as each SC requires its own controlled actuation unlike externally activated approaches.

In pick-and-place applications in industries and robotics, optimizing operation costs involves critical parameters such as response time, suction force, impact on the object, and energy consumption. In view of the two first parameters, externally activated SC is the most common choice. However, tons of energy have been consumed or wasted in SC applications. For instance, in 2012, vacuum generation alone consumed 0.8–3.2 TWh of energy in Germany.[20] Given the current environmental challenges and rising energy costs, reducing energy consumption in SC applications has become increasingly important. In addition to the energy unavoidably consumed by vacuum generators, primary energy waste occurs due to three main factors, which this article addresses. 1) Improper positioning of SCs on the workpiece surface or complex surface morphologies often leads to suboptimal sealing of the SC. The resulting leakage leads to an increase in pressure that is often compensated by the vacuum generator, which in doing so consumes more energy. 2) When using SCs in an array composition, unused SCs that are not in contact with the workpiece remain open, which also leads to significant vacuum loss that needs to be compensated by the vacuum generator. 3) Damages to SCs compromise their airtightness, again resulting in higher energy consumption.

Researchers have conducted studies to enhance the energy efficiency of SCs by optimizing their position and angle. An optimal attachment position or angle ensures better sealing on the object, thereby reducing the energy required to generate an equivalent adhesive force. But the dynamic evaluation of the vacuum gripper while moving objects is complex because of the simultaneous presence of tangential forces and torsional torques.[21,22] Advancements in dynamic simulation technology have allowed the consideration of workpiece surface roughness, curvature, as well as the number and diameter of SCs in grasp planning optimization.[23,24] Genetic algorithms and deep learning optimization methods have been utilized to predict suction effects and optimize grasping locations, leading to improved vacuum force and reduced energy consumption.[25,26] By employing computer vision and intelligent algorithms, energy consumption in SC deployment has been effectively reduced. However, this approach may result in heavier computational workloads, especially as more vacuum grippers aim for versatility in interacting with irregular objects and unknown environments.[27–30]

In addition to optimizing the position and angle of SCs, integrating contact-triggering functions has been explored to prevent energy waste in array configurations. Typically, sensors are incorporated into SCs to detect contact and trigger actuation.[31] However, this approach increases system complexity and requires additional energy for control. To address this, contact-triggered structures have been developed and integrated into SCs.[32,33] These structures feature a contact-triggered valve that controls the vacuum interface of each SC, allowing unused SCs to automatically close the vacuum interface and conserve energy. Tianqi et al. developed an adaptive SC with a rubber one-way duckbill valve and snap-through membrane for autonomous and energy-efficient grasping, utilizing a contact-triggered mechanism.[34] However, these designs are based on rigid valves, which may limit integration with soft robots like tentacle arms and grippers.[35–37] Another strategy involves improving airtightness on the object surfaces by employing film seals. The object is initially sucked up by a vacuum source, creating a sealed volume between the film and the object surface, resulting in a secondary vacuum effect.[38–41] These SCs exert higher force on rough surfaces due to improved airtightness and are compatible with smaller objects. However, their adaptability is accompanied by vulnerability. These SCs are more susceptible to damage due to the thin and soft films used in their construction.

In this article, we introduce a novel multi-material SC (MSC) with self-healing and self-closing capabilities. Our goal is to enhance energy efficiency in vacuum grippers equipped with SC arrays. The novel SC offers several improvements: i) a self-closing function based on a unique geometrical design that eliminates energy waste in SC arrays, ii) enhanced versatility and stability, reducing leakages between SCs and objects while stabilizing adhesive force through multi-material design, and iii) resilience, extending the operational lifespan and reducing repair costs by incorporating self-healing capacity (**Figure 1**). By integrating these functionalities, we enhance the physical intelligence (PI) of both the SCs and the overall system. In Section 2.1, we illustrate these new levels of artificial PI by comparing them to the biological PI of an octopus. Section 2.2 focuses on the multi-material composition of the SC, utilizing two reversible Diels–Alder (DA) polymers with distinct material properties. These polymers can be bonded without adhesive, forming high-strength multi-material interfaces through a heat–cool cycle. Tensile testing demonstrates the robustness of these interfaces, enabling the combination of hyper-flexible and stiff elastomers in a single SC design. This design offers versatility in picking up objects of various sizes and shapes while maintaining stability during movement. The SC's performance is characterized on a dedicated test bench and benchmarked against single-material SCs. Section 2.3 investigates the self-healing ability of the SC at both the material and system levels, subjecting it to macroscopic damage and subsequent healing under different conditions, such as room temperature and heating. The recovery of material properties and SC performance serves as an evaluation metric for healing effectiveness. Additionally, Section 2.4 presents the design and simulation

© 2023 The Authors. Advanced Intelligent Systems published by Wiley-VCH GmbH

26404567, 2023, 10, Downloaded from https://onlinelibrary.wiley.com/doi/10.1002/aisy.202300135 by EVIDENCE AID - BELGIUM, Wiley Online Library on [23/11/2023]. See the Terms and Conditions (https://onlinelibrary.wiley.com/terms-and-conditions) on Wiley Online Library for rules of use; OA articles are governed by the applicable Creative Commons License

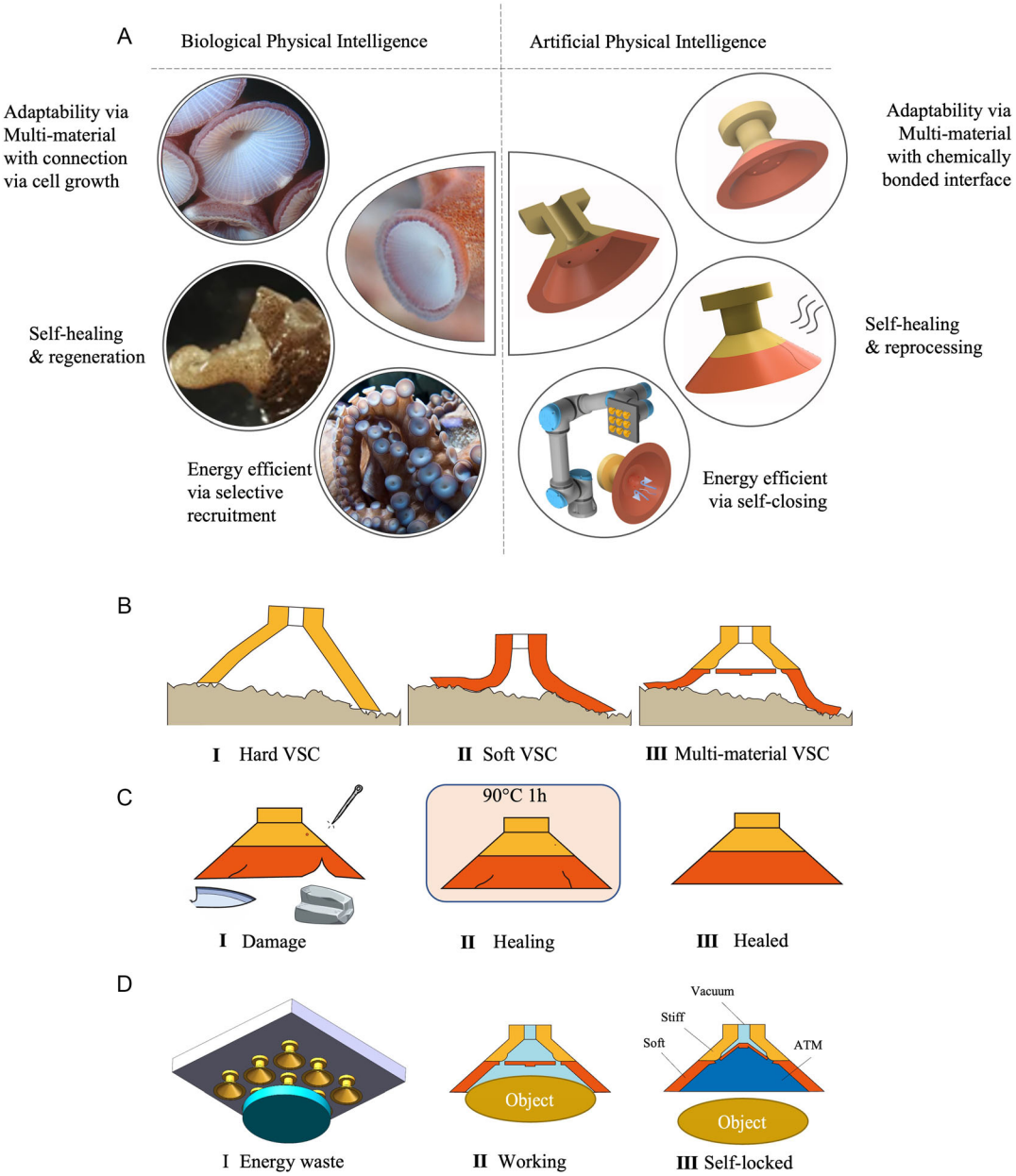

Figure 1. A) Overview of the self-healing, self-closing, and energy-efficient multi-material suction cups (MSC). A) Bioinspiration from octopus suction cups (SCs). The octopus regeneration image was reproduced with permission from ref. [44]. B) Multi-material structure combining adaptability and stability. I) The hard SC (HSC) cannot seal on irregular surfaces, II) the soft SC (SSC) is adaptive to irregular surfaces but with lower force caused by the smaller vacuum surface, and III) the MSC can keep the vacuum surface and adapt to irregular surfaces. C) Damages and self-healing of the SC. I) Damages such as puncture, cutting, and squeezing in the soft part of the MSC can be healed autonomously at room temperature in 24 h or in a single hour by heating to 80 °C. II) Damages in the stiff part of the MSC heal in 1 h by heating to 90 °C. III) The healed self-healing SC has no scar or weak point. D) Illustration of energy waste and self-closing mechanism. I) Vacuum leakage in the array of SCs, II) MSC attached to a workpiece, and III) MSC self-closed after releasing a workpiece.

of the self-closing system based on fluid-structure interaction finite-element analysis (FEA). The self-closing function is validated through benchmarking against a regular SC that lacks self-closing. Lastly, in Section 2.5, we introduce a novel approach for recycling multi-material elastomeric parts, including the MSC. This method utilizes the DA cross-links present in the reversible polymers and across the multi-material interface.

2. Results

2.1. Levels of PI

When designing SCs, it is difficult to overlook the inspiration provided by the octopus. This extraordinary creature showcases that intelligence is not solely dependent on computational intelligence (CI) but also on its PI. PI encompasses the incorporation

© 2023 The Authors. Advanced Intelligent Systems published by Wiley-VCH GmbH

26404567, 2023, 10, Downloaded from https://onlinelibrary.wiley.com/doi/10.1002/aisy.202300135 by EVIDENCE AID - BELGIUM, Wiley Online Library on [23/11/2023]. See the Terms and Conditions (https://onlinelibrary.wiley.com/terms-and-conditions) on Wiley Online Library for rules of use; OA articles are governed by the applicable Creative Commons License

of sensing, actuation, control, memory, logic, computation, adaptation, learning, and decision-making within the body of an organism or artificially created machine (agent).[42]

2.1.1. PI via Structural Intelligence

Even when freshly amputated, octopus tentacles can still adhere to objects, highlighting that the grasping function is achieved through PI rather than central CI. Despite having a total of 2240 SCs, octopuses possess precise tactile control over their suckers and can individually recruit them with efficiency. In array configurations commonly found in industrial applications (Figure 1A), individual recruitment is mostly impossible. Consequently, extensive air losses occur when grasping objects that do not cover the entire array. While selective recruitment has been explored, it typically relies on active and bulky systems that involve costly components such as sensors, actuators, and control mechanisms, thereby reducing payload capacity. In this article, we present a groundbreaking concept: a passive and soft self-closing principle that can be directly embedded into SCs without altering their dimensions. Within an array configuration, only SCs in contact with objects are selectively recruited, while the remaining SCs are sealed off, preventing any undesired airflow that could hinder overall performance and efficiency. This self-closing functionality is entirely passive and does not require computation or control mechanisms.

2.1.2. PI via Multi-Material Composition

The octopus, despite its soft nature, consists of a variety of materials with diverse mechanical properties. Researchers have demonstrated that the infundibulum, the contact area of the octopus's SC, is one of the softest biological materials (7.7 kPa).[43] This extreme softness enables excellent contact with any surface, making the octopus highly versatile in grasping objects of various types. The soft infundibulum is connected to a less flexible tentacle through cell growth. Similarly, in this article, we leverage the combination of a hyper-flexible elastomer (120 kPa) and a stiff elastomer (54 MPa) in the multi-material design of a versatile SC. Multi-material designs are often avoided in industries due to the vulnerability of multi-material interfaces. Over time, stress concentrations at the interface, relying solely on weak secondary interactions (adhesion), can lead to delamination and failure of the multi-material parts. Specifically, combining materials with significant differences in moduli poses greater challenges. To overcome this obstacle, we employ reversible elastomers cross-linked by thermoreversible DA bonds. Through a heat–cool cycle, two DA polymers with distinct mechanical properties (with a difference of three orders of magnitude in Young's modulus) are chemically bonded together, resulting in a high-strength multi-material interface that mirrors the strength found in biologically grown multi-material systems within the octopus's body. This unique capability of reversible polymers enables the realization of multi-material designs with enhanced PI capabilities.

2.1.3. PI via Self-Healing and Recyclable Polymers

Octopuses possess remarkable regenerative abilities, being able to quickly recover from severe wounds and regrow a lost tentacle in just 2–4 months.[44] This biological healing capacity has inspired scientists to develop synthetic self-healing polymers. In this article, we introduce a synthetic healing ability in SCs by manufacturing them out of reversible elastomers that contain DA bonds, providing healing capabilities (**Figure 2**). When damaged, such as by puncture, tear, or cut, the DA bonds at the site of damage are mechanically broken, resulting in the formation of reactive maleimide and furan groups. Upon reuniting the fractured surfaces, these reactive groups react to reform the broken DA bonds, initiating the healing process. This healing occurs at room temperature within approximately a day, and it can be expedited by applying mild heating (80–90 °C), reducing healing time to just 1 h. Following healing, the initial mechanical properties are fully restored, allowing for an infinite number of damage-healing cycles. In this study, the MSC is entirely composed of self-healing polymers. This inherent self-healing capability eliminates air losses due to damage, enabling SCs to be designed based on their intended functionality rather than accounting for potential damage. This approach allows for more lightweight and compact SC designs by avoiding excessive safety factors. Additionally, enhancing the lifespan of SCs through healing is both cost-efficient and sustainable. Moreover, the DA bonds can be thermally broken, causing the polymeric network to transition into a viscous liquid state at higher temperatures. This property offers the possibility of reprocessing and recycling the materials, which stands in stark contrast to traditional elastomers used in SCs that are irreversibly cross-linked and cannot be reprocessed. Both healing and recycling will play crucial roles in developing sustainable SCs for the future.

2.2. MSC

2.2.1. Design and Material Composition

When designing SCs, choosing the appropriate material poses a challenging decision (Figure 1B I and II). Opting for stiff elastomers allows for SCs capable of generating high adhesive forces, particularly on smooth surfaces. Additionally, the increased stiffness contributes to more stable grasping during gripper movement. On the other hand, SCs made from hyper-flexible elastomers have the ability to achieve vacuum sealing on rough and irregular surfaces.[45] However, their adhesive force and stability are limited due to the uncertainty surrounding the vacuum area within the SC chamber. To be effective in industrial or service robot applications, SCs must strike a balance between stability, high adhesion, and versatility. Vacuum grippers are expected not only to grasp a variety of objects but also to securely hold and move them, avoiding any potential damage caused by releasing the object due to shaking or imprecise movements.

The proposed MSC, consisting of stiff and hyper-flexible elastomers, combines the advantages of both hyper-flexible and stiff SCs (Figure 1B III). The basic geometry of the SC is based on existing designs from the literature (**Figure 3**A I), as this paper primarily focuses on improving embodied intelligence through novel materials, multi-material composition, and a self-closing function, rather than through geometric design. Nonetheless, the findings presented are applicable to a wide range of geometrical SCs, including bellow SCs (Supporting Information). The MSC is constructed entirely from two

© 2023 The Authors. Advanced Intelligent Systems published by Wiley-VCH GmbH

26404567, 2023, 10, Downloaded from https://onlinelibrary.wiley.com/doi/10.1002/aisy.202300135 by EVIDENCE AID - BELGIUM, Wiley Online Library on [23/11/2023]. See the Terms and Conditions (https://onlinelibrary.wiley.com/terms-and-conditions) on Wiley Online Library for rules of use; OA articles are governed by the applicable Creative Commons License

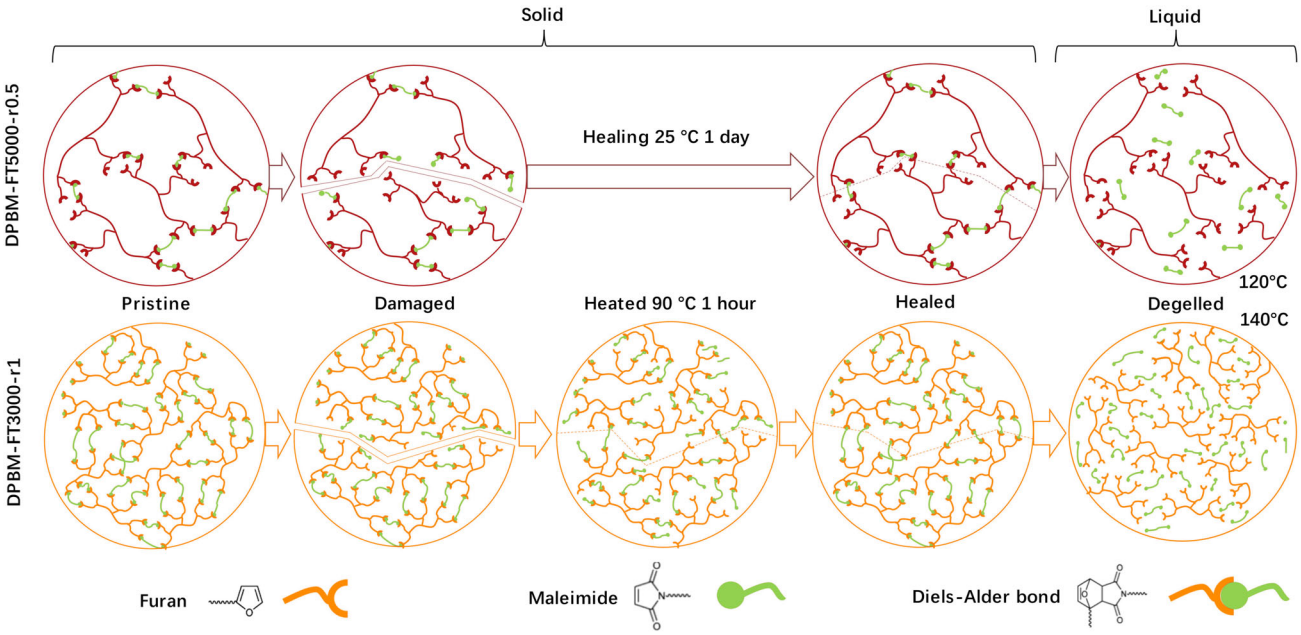

Figure 2. Schematics of the self-healing process in Diels–Alder (DA)-based reversible elastomers. Depending on the materials initial molecular mobility, the healing is autonomous at ambient conditions or requires a temperature elevation to reach desired mobility levels. Heating the network polymer above its degelation temperature leads to a solid to liquid transition completely reversible upon cooling.

elastomeric polymers with distinct mechanical properties. The upper yellow neck section is composed of hard DPBM-FT3000-r1, possessing a Young's modulus of 54 MPa to provide stiffness and strength. The lower red suction chamber is made of hyper-elastic DPBM-FT5000-r0.5, with a Young's modulus of 0.12 MPa and a strain capability exceeding 250%, ensuring versatility in grasping objects with various shapes. The difference in mechanical properties between the two elastomers is demonstrated through tensile testing at a rate of 1% s^{-1} (Figure 3B).

2.2.2. High Strength Multi-Material Interface

Interfaces between materials with divergent mechanical properties, often found in soft devices like soft robotics and flexible sensors, tend to be critical areas where failures occur due to limited lifetimes. This is attributed to stress concentrations at the interface and weak adhesion between the parts, leading to delamination. One advantage of reversible elastomers is their ability to seamlessly connect two elastomers with distinct mechanical properties through high-strength multi-material interfaces.[46,47] The upper DPBM-FT3000-r1 part (yellow) and the lower DPBM-FT5000-r0.5 part (red) of the MSC were manufactured using casting methods (Supplementary Materials 1, Supporting Information). These parts were joined together via a heat–cool cycle while remaining in the solid state. After bringing the top and bottom parts into contact, the assembly was heated at 90 °C for one hour. At this elevated temperature, the DA reaction equilibrium shifted toward the unbound state, reducing the number of DA crosslinks and creating reactive furan and maleimide groups. Subsequently, the assembly was cooled to room temperature and left for 24 h. At this lower temperature, the reaction equilibrium shifted toward the bound state, restoring a large number of DA crosslinks within the elastomeric network and across the multi-material interface. The result is a robust, chemically bonded multi-material interface in the MSC. This covalent bonding provides a significant contrast to the adhesive interfaces typically used in multi-material product assembly, which depend on weaker secondary (non-covalent) interactions.

The strength of the multi-material interface was assessed through tensile testing of multi-material samples (Figure 3C, $30 \times 5 \times 1\ mm^3$). These samples were produced using the aforementioned heat–cool cycle and subjected to a tensile test until fracture at a rate of 1% s^{-1}. The results were compared to fracture tests conducted on pure DPBM-FT3000-r1 and DPBM-FT5000-r0.5 samples. The block diagram in Figure 3B illustrates that the multi-material samples exhibit higher fracture stresses compared to the most flexible DPBM-FT5000-r0.5 material, indicating a robust interface. Visual examination of the fracture using a digital camera further confirms this, as the fracture in the multi-material samples occurs within the region of the most flexible and weakest material, DPBM-FT5000-r0.5, rather than at the interface (Figure 3B). This innovative approach for connecting multi-material parts presents exciting possibilities for creating durable multi-material components, scalable even to miniaturized components. It eliminates the need for adhesives or reliance on geometric design for connecting parts.

2.2.3. Combining Versatility and Stability

To demonstrate the synergistic combination of versatility and stability achieved by incorporating multiple materials in the MSC,

© 2023 The Authors. Advanced Intelligent Systems published by Wiley-VCH GmbH

26404567, 2023, 10, Downloaded from https://onlinelibrary.wiley.com/doi/10.1002/aisy.202300135 by EVIDENCE AID - BELGIUM, Wiley Online Library on [23/11/2023]. See the Terms and Conditions (https://onlinelibrary.wiley.com/terms-and-conditions) on Wiley Online Library for rules of use; OA articles are governed by the applicable Creative Commons License

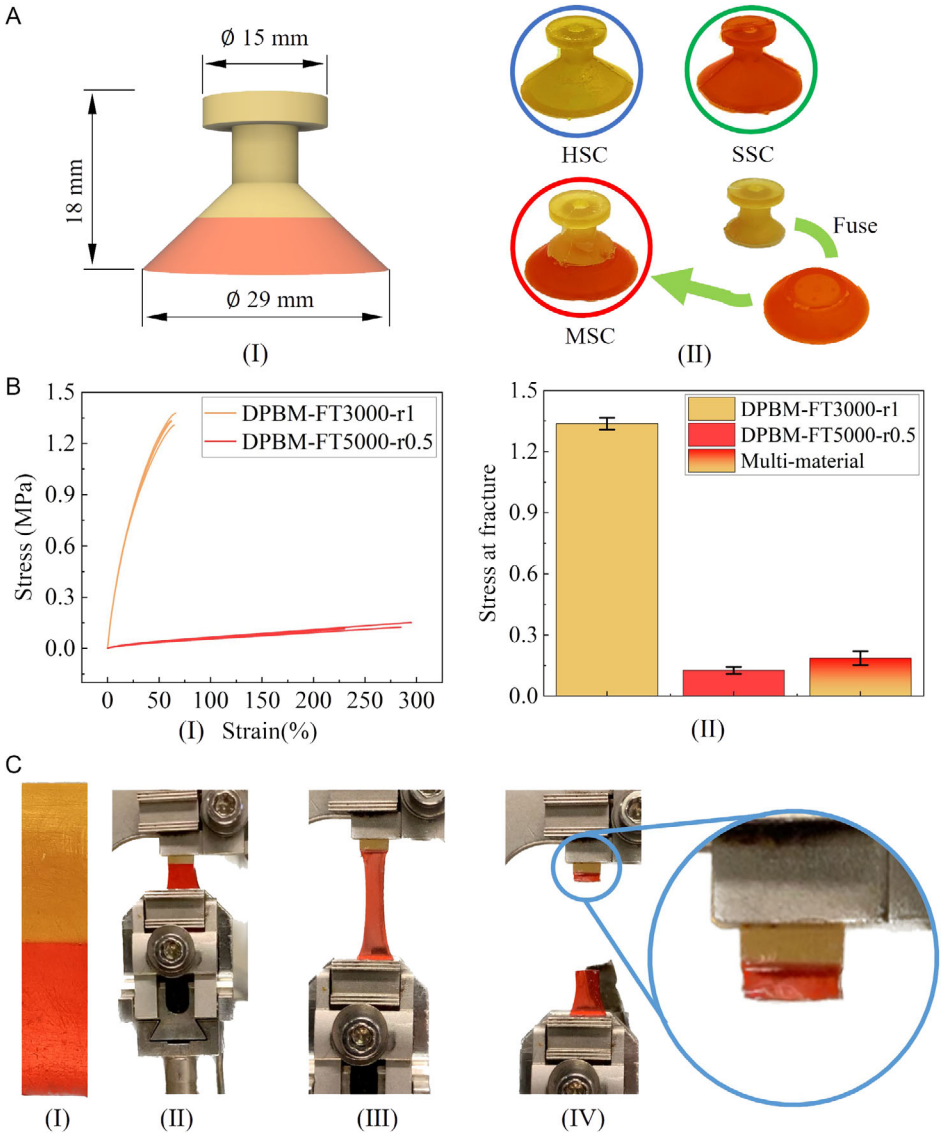

Figure 3. MSC fabrication and material characterization. A) I) The exterior dimensions of the MSC. II) The methodology of fabricating the MSC casts the hard and the soft parts separately, and then fused them together with the DA reaction. B) I) The tensile tests for DPBM-FT3000-r1 and DPBM-FT5000-r0.5. II) The stress at fracture for pure materials and the bonded multi-material in tensile tests, showing the interface of multi-materials does not reduce the strength. C) The sample of multi-material made by bonding DPBM-FT3000-r1 and DPBM-FT5000-r0.5 (I—it was clamped on the tensile test machine; II—the elongation mostly located in the DPBM-FT5000-r0.5; and III—it always fractured in the DPBM-FT5000-r0.5, IV—rather than the interface between two materials).

its performance was compared against two SCs made solely from pure DPBM-FT3000-r1 or DPBM-FT5000-r0.5 elastomers (Figure 3A). The SC composed entirely of stiff DPBM-FT3000-r1 elastomer was denoted as the hard SC (HSC), while the one solely constructed from highly flexible DPBM-FT5000-r0.5 was referred to as the soft SC (SSC). Utilizing more flexible materials for the suction chamber enhances the SC's versatility in grasping objects with varying roughness and geometry. However, the increased flexibility of the SSC comes at the expense of stability when subjected to external forces, such as those encountered when the SC moves or rotates an object as an end-effector on a robotic manipulator.

The MSC, HSC, and SSC underwent characterization on a dedicated test bench equipped with a tensile device (Tinius Olsen 5ST) and a pressure controller (**Figure** 4B). The maximum adhesive force, representing the force at detachment of the SC, was measured across a range of pressures (−10 kPa to −80 kPa) on three different surfaces: flat, concave, and convex (all with a 30 mm radius). Additionally, the maximum adhesive force was measured in the lateral direction on a flat surface. Figure 4A shows the maximum adhesive force plotted as a function of vacuum pressure. The HSC demonstrated higher adhesive force due to its stiffness, which allows for a larger vacuum area to be retained, except for pressures below −20 kPa where the HSC cannot

© 2023 The Authors. Advanced Intelligent Systems published by Wiley-VCH GmbH

26404567, 2023, 10, Downloaded from https://onlinelibrary.wiley.com/doi/10.1002/aisy.202300135 by EVIDENCE AID - BELGIUM, Wiley Online Library on [23/11/2023]. See the Terms and Conditions (https://onlinelibrary.wiley.com/terms-and-conditions) on Wiley Online Library for rules of use; OA articles are governed by the applicable Creative Commons License

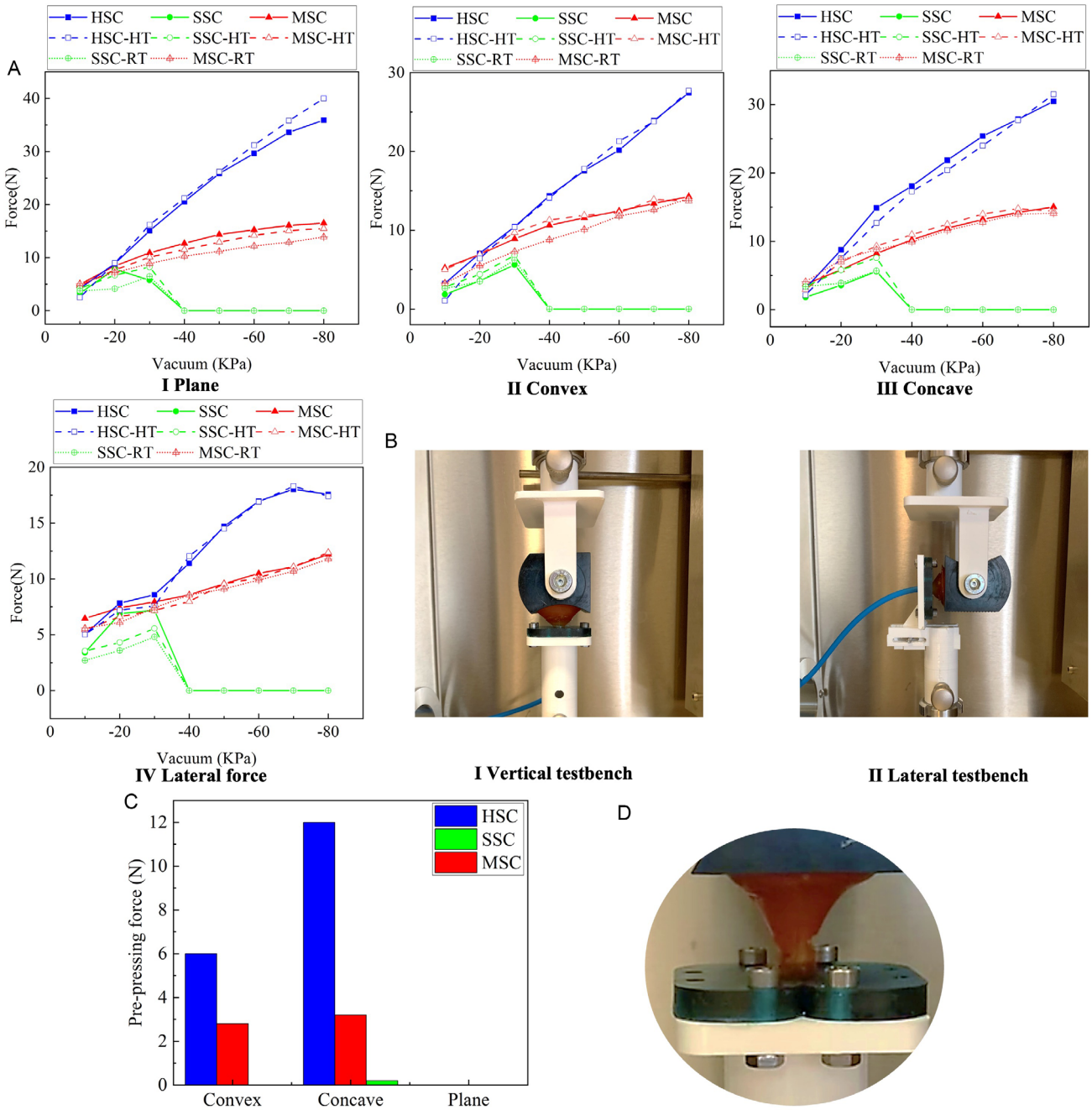

Figure 4. Adhesive force measurements for SCs. A) Axial and lateral adhesive force tests. Solid curves, dash curves, and dot curves show data for pristine, heating-healed, and room-temperature-healed SCs. I) Tensile tests in case of SCs attach on a plane surface, II) tensile tests in case of SCs attach on a convex surface with curvature radius 30 mm, III) tensile tests in case of SCs attach on a concave surface with curvature radius 30 mm. IV) Lateral tensile tests in case of SCs attach on a plane surface. B) Test benches for adhesive force measurements: I) vertical adhesive force tests, and II) lateral adhesive force tests. C) Required pre-pressing force to generate effective vacuum chambers sealing on the different surfaces. D) The fracture failure of the SSC.

deform sufficiently to form an airtight seal on surfaces. In the SSC, the vacuum area is reduced due to the deformation of the cup, leading to lower forces. However, even more catastrophic is the damage that occurs in the neck of the SSC when performing the tests at vacuum pressures below −30 kPa (Figure 4D). In comparison, the MSC demonstrated higher adhesion force before detachment, surpassing the SSC, and remained intact. This demonstrates that using stiffer materials for the top part of the SC is necessary not only for stability but also for strength.

The pressing force necessary to establish proper contact between the SC and the object is another crucial parameter to consider. The minimum pressing force required to create a vacuum was recorded for each surface type (flat, concave, and convex) and each SC, and the results are illustrated in

© 2023 The Authors. Advanced Intelligent Systems published by Wiley-VCH GmbH

26404567, 2023, 10, Downloaded from https://onlinelibrary.wiley.com/doi/10.1002/aisy.202300135 by EVIDENCE AID - BELGIUM, Wiley Online Library on [23/11/2023]. See the Terms and Conditions (https://onlinelibrary.wiley.com/terms-and-conditions) on Wiley Online Library for rules of use; OA articles are governed by the applicable Creative Commons License

Figure 4C. On a flat surface, the pressing force is negligible. However, the HSC demands higher forces to achieve effective sealing on curved surfaces. This parameter becomes increasingly significant when handling fragile objects and can play a pivotal role in preventing any damage to the objects.

The SCs were integrated as end-effectors on a robotic manipulator, specifically the Rotrics DexArm (**Figure 5**A). Initially, the maximum vacuum pressure required to lift a 338 g orange was determined for each SC and presented in Figure 5D. The HSC necessitated a higher vacuum due to the orange's rough surface, resulting in increased energy consumption. To assess grasp stability, the orange's movement was tracked using a digital camera while being horizontally displaced at a velocity of 83 mm s^{-1} and abruptly stopped. Figure 5E demonstrates the displacement between the tracking point (middle of the orange) and the robot head, providing an indicator of orange shaking (Figure 5B). When employing the HSC, the displacement after an abrupt stop remained negligible, indicating minimal orange shaking. Conversely, when utilizing the SSC, the orange continued to exhibit prolonged shaking with relatively large displacements

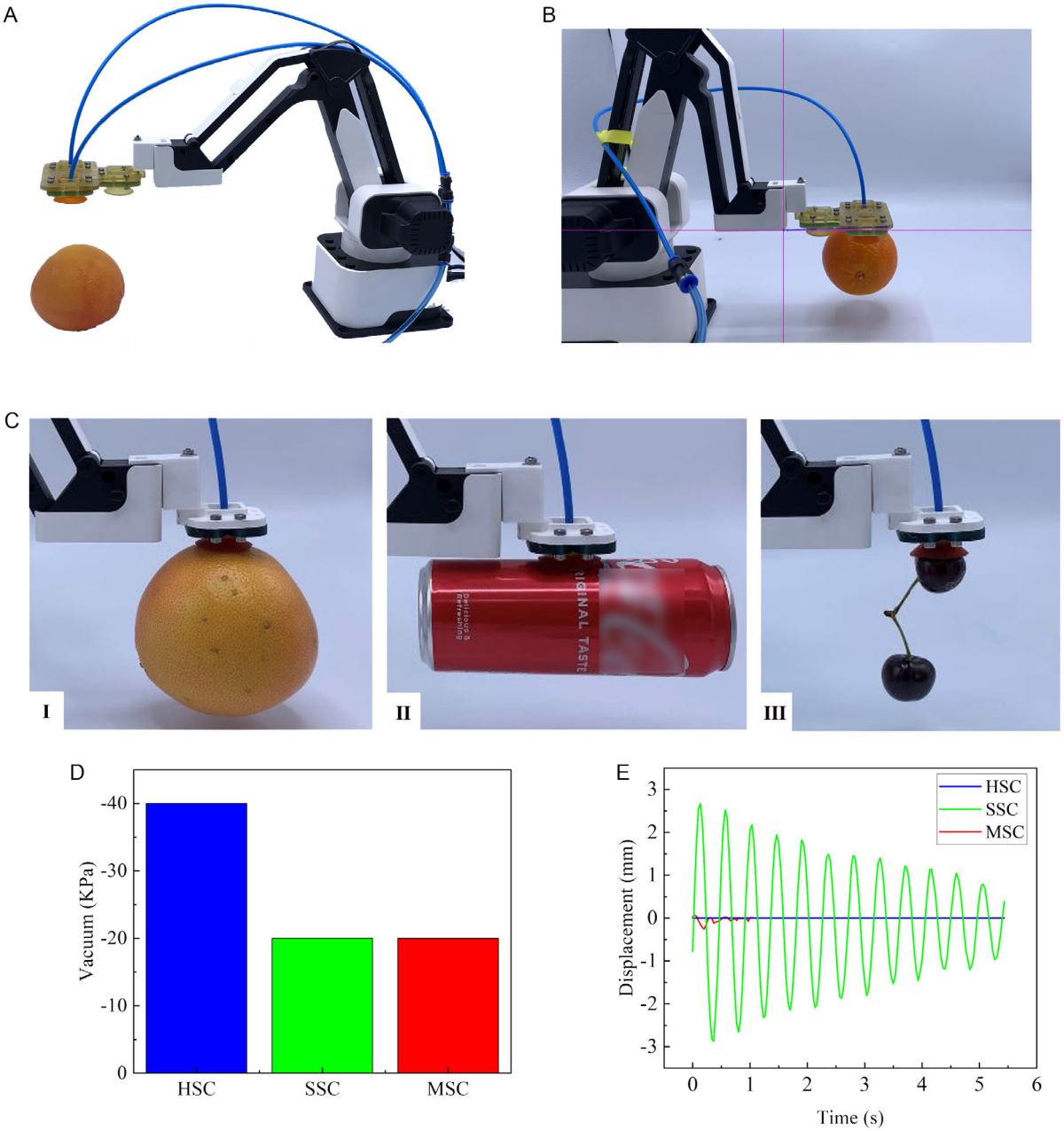

Figure 5. The versatility and stability demonstration of the MSC. A) SCs are mounted on a robot arm to pick up a 338 g orange for comparing the adhesive difference on the rough surface. B) Track the shake of the orange when the robot arm moves it and stop. C) I) The MSC picks up an orange; II) an aluminum can full of liquid, and III) cherries. D) The consumed vacuum for picking up the orange, HSC requires a higher vacuum to compensate for the leakage between the SC and the orange surface. E) The shake of SCs when they stop moving a 338 g orange from horizontal movement of 83 mm s^{-1}.

© 2023 The Authors. Advanced Intelligent Systems published by Wiley-VCH GmbH

26404567, 2023, 10, Downloaded from https://onlinelibrary.wiley.com/doi/10.1002/aisy.202300135 by EVIDENCE AID - BELGIUM, Wiley Online Library on [23/11/2023]. See the Terms and Conditions (https://onlinelibrary.wiley.com/terms-and-conditions) on Wiley Online Library for rules of use; OA articles are governed by the applicable Creative Commons License

starting at 2.5 mm. The MSC exhibited only minimal shaking. For applications in industries that necessitate precise and rapid pick-and-place operations, this operational stability is critical.

In summary, the MSC offers a unique combination of hard and soft materials that enables the integration of high adhesive forces with minimal pressing forces on the object, facilitated by excellent contact. The spatial arrangement of polymers with distinct elastic moduli empowers the SC to efficiently lift rough-surfaced objects using low vacuum power while ensuring swift and stable movement. As depicted in Figure 5C, the MSC successfully grasps small, irregular cherries without causing damage, whereas the HSC fails in this task. It also demonstrates the ability to securely hold a liquid-filled aluminum can, which experiences significant shaking when handled by the SSC. Moreover, the MSC effectively lifts a large orange with a visibly rough surface. The spatial distribution of hard and soft elastomers can be further tailored to suit different applications or objects. Increasing the proportion of relatively stiff material enhances adhesive force while reducing flexibility, and vice versa. Additionally, the mechanical properties of reversible elastomers can be fine-tuned by adjusting polymer network design parameters to optimize performance for specific applications.[48,49]

2.3. Self-Healing Ability

2.3.1. Self-Healing on the Material Level

For the SC's damage-healing ability to be economically valuable, it must effectively heal relevant macroscopic damages, such as cuts, perforations, and tears caused by sharp objects or fatigue (Figure 1C I). Damages leading to air leaks result in pressure increases that need to be compensated by the pressure controller, leading to energy wastage. The DA crosslinks in both reversible elastomers, DPBM-FT5000-r0.5 and DPBM-FT3000-r1, enable the integration of healing capacity within the SC. In the highly flexible DPBM-FT5000-r0.5, healing occurs autonomously under ambient conditions, such as room temperature (around 25 °C), within 24 h. The material's softness facilitates excellent molecular-level contact when the fracture surfaces are reconnected. However, the stiffer DPBM-FT3000-r1 material does not heal at room temperature and requires a temperature increase to 90 °C for 1 h to enhance mobility in the reversible network (Figure 1C II III). At 90 °C, the equilibrium of the DA reaction shifts toward the unbound state, reducing crosslink density and increasing mobility. The reaction kinetics of the DA reaction also accelerates at higher temperatures, resulting in faster bonding of the DA bonds across the fracture surfaces. As a result, higher temperatures reduce healing time. This is similarly observed for the DPBM-FT5000-r0.5 material, which heals within just 1 h at 80 °C.

The self-healing ability is experimentally validated by conducting tensile testing on pure DPBM-FT5000-r0.5 and DPBM-FT3000-r1 samples with dimensions of $30 \times 5 \times 1\ mm^3$ dimensions (**Figure 6**A). The samples are cut in half and manually brought back into contact. Subsequently, they are either healed at room temperature or subjected to healing at 80 or 90 °C in a preheated oven. To assess the healing of DPBM-FT5000-r0.5, the samples are fractured in a tensile test at a rate of 1% s^{-1} after 5 min, 40 min, or 24 h at room temperature, or after 1 h at 80 °C. The resulting stress-strain curves are compared with those of an undamaged, pristine sample (Figure 6B I). The healing efficiencies are calculated based on the recovery of fracture stress, fracture strain, toughness, and Young's modulus, which is determined through linear regression in the 0%–15% strain range (Figure 6B III). The healing efficiency is defined as the ratio between the property measured after healing and the property of the pristine sample. Within just 5 min of healing at room temperature, the mechanical properties are partially recovered for low strains up to 25 °C. However, at higher strains, the mechanical behavior deviates from the pristine behavior, and the sample fractures at a limited strain of 80%. This indicates that a fraction of the DA bonds is reformed across the fracture surfaces within minutes, facilitated by excellent contact. After 40 min at 25 °C, the mechanical properties are significantly improved and nearly identical to the pristine behavior, withstanding strains of up to 85% before fracture. Following 24 h of healing at 25 °C, the full mechanical performance is almost entirely restored, resulting in healing efficiencies of 92%, 94% and 89% for fracture strain, fracture strain recovery, and toughness, respectively. However, the fracture still occurs at the location of the healed damage, referred to as the scar.

Heating during the healing process not only accelerates healing speed but also enhances recovery, as demonstrated by the results of the DPBM-FT5000-r0.5 sample healed at 80 °C for one hour. Within just one hour, the fracture stress, fracture strain, and toughness are recovered at rates of 102%, 102%, and 103%, respectively. Notably, failure occurs at locations distinct from the scar, indicating that damage-healing does not introduce weak spots in the material. This perfect recovery is attributed to the elimination of the scar through heating, as observed in the microscopic images in Figure 6A. At elevated temperatures, increased molecular mobility facilitates improved sealing and the elimination of microscopic misalignments that occur when the fracture surfaces are brought into contact. Rectifying these geometric effects leads to complete recovery. As previously mentioned, the stiffer DPBM-FT3000-r1 does not heal at 25 °C. However, samples healed at 90 °C for 1 h exhibit exceptional recovery, with healing efficiencies of 100%, 105% and 105% for fracture strain, fracture strain recovery, and toughness, respectively (Figure 6B II III).

2.3.2. Self-Healing on the System Level

The healing capacity of the SCs, including the HSC, SSC, and MSC, is investigated at the cup level. Manual punctures and cuts are made using a needle and scalpel blade, respectively (Figure 6E). The elastic recovery of the elastomeric material allows the fracture surfaces to regain contact, both in the stiff DPBM-FT3000-r1 and the soft DPBM-FT5000-r0.5. This self-sealing ability enables autonomous healing without human intervention. Initially, room temperature healing is examined by leaving the SCs at 25 °C for 24 h. The recovery is assessed by investigating the maximum adhesion force as a function of vacuum pressure (Figure 4A). In the HSC, damages in the stiff DPBM-FT3000-r1 material cannot be healed without the application of heat. However, damages in the soft DPBM-FT5000-r0.5 material exhibit full recovery in this timeframe, as observed in the MSC and SSC (Figure 6E). Although scars are still visible (Figure 6E III), the complete restoration of force demonstrates

© 2023 The Authors. Advanced Intelligent Systems published by Wiley-VCH GmbH

26404567, 2023, 10, Downloaded from https://onlinelibrary.wiley.com/doi/10.1002/aisy.202300135 by EVIDENCE AID - BELGIUM, Wiley Online Library on [23/11/2023]. See the Terms and Conditions (https://onlinelibrary.wiley.com/terms-and-conditions) on Wiley Online Library for rules of use; OA articles are governed by the applicable Creative Commons License

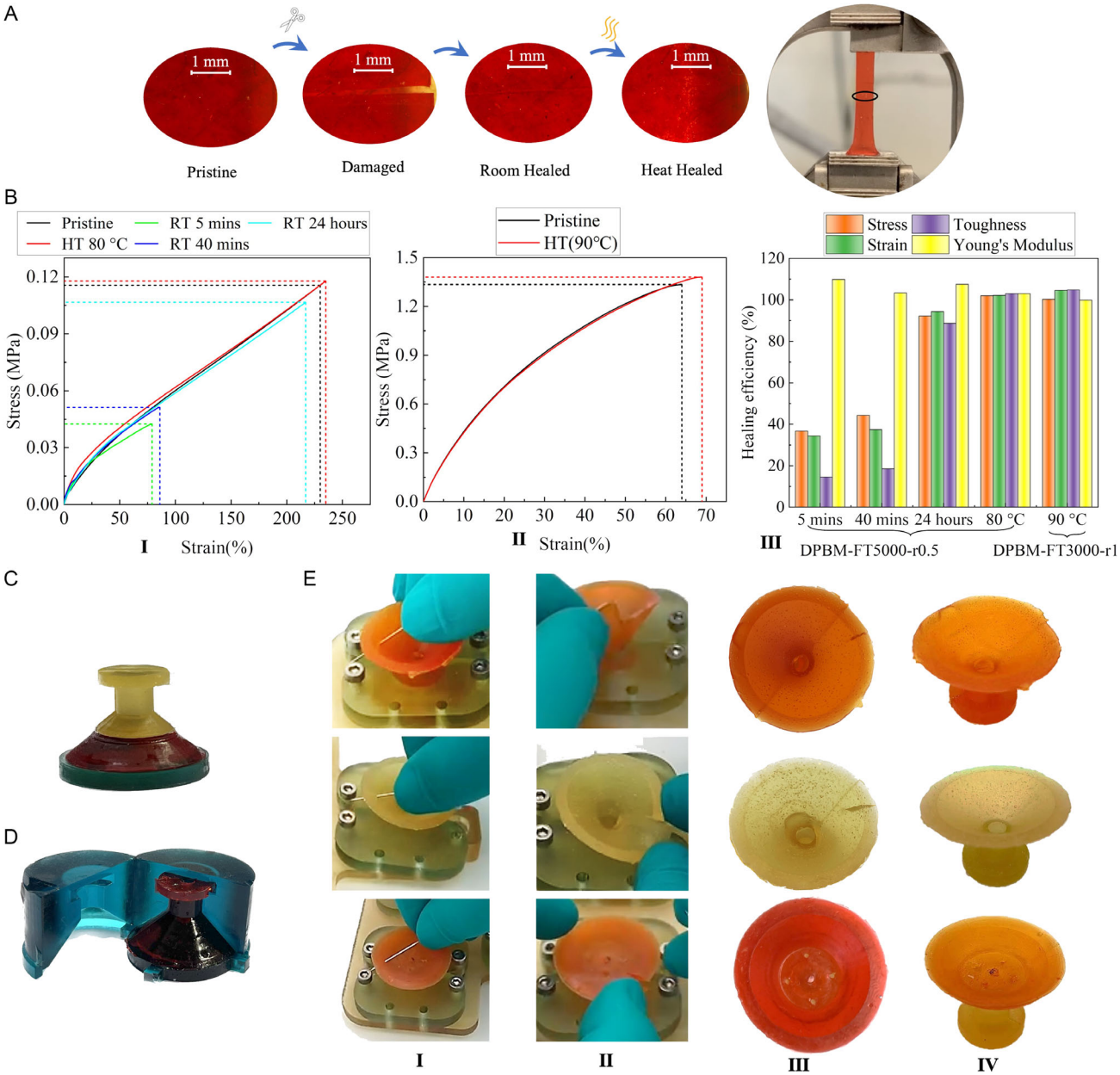

Figure 6. Self-healing tests on materials and SCs. A) DPBM-FT5000-r0.5 was cut and then brought back in contact to heal. The samples that healed at room temperate still have slightly visible scars, the samples healed by heating without scars. The scar was clearer during tensile tests. B) I) The stress–strain curves of the DPBM-FT5000-r0.5 that healed at room temperature for 5 min, 40 min, and 24 h, and healed at 80 °C for 1 h, compared to the pristine property. II) The stress–strain curves of the DPBM-FT3000-r1 healed at 90 °C for 1 h and the pristine property. III) The healing efficiency at different conditions is characterized by stress and strain at fracture, Young's modulus, and toughness. C) The MSC is put on bottom support to heal the wound on the hard part. D) The SSC is put in the mold for healing without a scar. E) SCs are I) punctured and II) cut, and III) then healed at room temperature for 24 h; the MSC has minimal visible scar while the HSC cannot heal. IV) All the SCs heal without scars by heating healing.

that the SCs are healed without leakage. Notably, the SSC exhibits a more prominent scar compared to the MSC. This discrepancy is attributed to the stiffer self-healing material's superior elastic response and resistance against deformation caused by gravitational forces. Consequently, the MSC with a more elastic top part facilitates enhanced shape recovery and self-sealing, resulting in improved healing.

Healing at room temperature can be time-consuming, and in certain applications, a 24 h downtime may not be acceptable. However, the healing process can be significantly accelerated by raising the temperature. Heating the SCs to 80 °C reduces the healing time to just 1 h for the DPBM-FT5000-r0.5, as evidenced by the recovery of the maximum adhesion force in the SSC and MSC (Figure 4A). It is important to note that the soft

© 2023 The Authors. Advanced Intelligent Systems published by Wiley-VCH GmbH

26404567, 2023, 10, Downloaded from https://onlinelibrary.wiley.com/doi/10.1002/aisy.202300135 by EVIDENCE AID - BELGIUM, Wiley Online Library on [23/11/2023]. See the Terms and Conditions (https://onlinelibrary.wiley.com/terms-and-conditions) on Wiley Online Library for rules of use; OA articles are governed by the applicable Creative Commons License

DPBM-FT5000-r0.5 material experiences some loss of structural integrity at this temperature, as it is close to its degelation temperature of 92 °C. As a result, the SSC had to be placed in a mold during the healing procedure (Figure 6D). In the case of the SSC, this healing procedure not only completely healed the punctures, cuts, but also successfully repaired the torn neck on four separate occasions (Figure 4D). Conversely, the MSC, with its stiff DPBM-FT3000-r1 top part, maintained structural stability throughout the healing process, eliminating the need for a mold. Consequently, the MSC can fully recover its performance after 1 h at 80 °C without requiring a mold.

Heating is also effective for healing the stiff DPBM-FT3000-r1, but it requires a temperature increase to 90 °C for a total duration of one hour. This higher temperature is necessary because the DPBM-FT3000-r1 does not heal within a reasonable time frame at 80 °C. The HSC exhibits full recovery following this healing procedure (Figure 4A). Similarly, damages in the stiff DPBM-FT3000-r1 of the MSC can also be healed. However, due to the proximity of 90 °C to the degelation point of DPBM-FT5000-r0.5, the bottom part of the MSC cannot maintain its form stability during this healing process, requiring the use of a bottom support during healing (Figure 6C). Nonetheless, after mold-assisted healing at 90 °C for 1 h, the MSC also regains its full performance following this type of damage (Figure 4A).

Depending on the application, the MSC offers two options for healing damage to the SC: room temperature healing and accelerated heated healing. Given that the soft part of the MSC is more susceptible to damage, both healing methods can be utilized. Room temperature healing enables autonomous healing without the need for additional stimulus, allowing for direct integration into existing systems. However, this healing process takes a full day. On the other hand, heated healing only requires 1 h, which can be achieved by placing the SC in a heated environment such as an oven, or by incorporating embedded heaters within the system.[50] In the event of damage occurring in the stiff region, mold-assisted healing provides a viable solution.

2.4. Self-Closing SC

In suction array grippers, energy wastage often occurs when SCs are not in contact with the grasped object (Figure 1D). While arrays of SCs are valued for their versatility in gripping various objects, they tend to leak when not in direct contact. This inefficiency not only reduces the vacuum and resulting suction force in active SCs (those in contact with the object), but also leads to energy waste. To address this issue, this paper proposes a solution by incorporating structural intelligence into the SC design. A soft passive self-closing valve is integrated, allowing the vacuum gripper to function like typical SCs when attached to objects (Figure 1D II), while effectively sealing the vacuum when not in contact (Figure 1D III). This self-closing feature eliminates energy waste caused by inactive SCs.

2.4.1. Self-Closing Mechanism

The self-closing feature of the MSC is achieved through the deformation of a film located in the neck of the gripper, which consists of four 1 mm diameter orifices (holes) (**Figure 7**C). When the vacuum source is activated, the air-pressure difference across the film increases due to the restricted airflow through the small orifices (Figure 7A,B). Consequently, the film bends and deforms toward the inner wall of the neck, effectively sealing the four holes and halting the airflow. To enhance the sealing process, a ring structure (Figure 7C, R2) is integrated into the design. When the gripper makes contact with an object, there is no airflow or pressure gradient inside the SC. Hence, the film remains in its original position without affecting the gripper's operation. The film is produced out of a highly flexible material, e.g., DPBM-FT5000-r0.5, as this increases the sensitivity of the sheet to the pressure difference.

2.4.2. Design and Simulation

The sensitivity of the self-closing system, which determines the minimum pressure difference required to seal the holes in the film (Figure 7C), is influenced by several parameters. These parameters include the z-position of the film (related to the film's radius), the number and radius of the holes (R3), the hole positions in the film (R4), the film's flexibility and thickness, and the radius of the ring structure (R2). The desired sensitivity level depends on the specific application. When working with irregular or rough surfaces, it is inevitable to have small gaps between the SC body and the surface. Thus, the self-closing system cannot be overly sensitive, as even a slight pressure difference caused by these gaps could trigger undesired closure of the SC. This interference would hinder the gripper's normal operation, making it unable to grasp objects. However, the sensitivity should still be sufficiently high to enable self-closing when the gripper is not in contact with an object. The design is correlated with the applied negative pressure, which in this study is set at a minimum of −30 kPa.

In this study, the flexibility of the self-closing system was determined based on the mechanical properties of the soft DPBM-FT5000-r0.5 material, which has a Young's modulus of 0.12 MPa. Sensitivity can be enhanced by reducing the film thickness, but the thickness is constrained by the film's strength requirement to withstand the vacuum. In order to resist negative pressures of −80 kPa, a minimum thickness of 0.8 mm is necessary. The film's strength is also influenced by the number of holes, which was fixed at four in this paper. The z-position of the film was set at 5.4 mm, resulting in a hole placement at a distance of 4.6 mm (R4) from the symmetrical axis. The choice of a 0.5 mm height was made to align with the multi-material interface in the MSC, facilitating manufacturing. Increasing the z-position would significantly enhance sensitivity as it reduces the deformation space between the film and the tube. However, lowering the z-position excessively could lead to interference or damage from the grasped object.

Subsequently, fluid-structure interaction simulations were conducted using COMSOL Multiphysics (Figure 7A) to investigate the impact of varying the radius of the four holes (R3) and the radius of the ring structure (R2 in Figure 7C). The simulations considered the two reversible elastomers, DPBM-FT5000-r0.5 and DPBM-FT3000-r1, modeled as linear elastic materials with Young's moduli of 0.12 and 54 MPa, respectively. The radius of the holes was varied from 0.5 to 1.5 mm, considering that a

© 2023 The Authors. Advanced Intelligent Systems published by Wiley-VCH GmbH

26404567, 2023, 10, Downloaded from https://onlinelibrary.wiley.com/doi/10.1002/aisy.202300135 by EVIDENCE AID - BELGIUM, Wiley Online Library on [23/11/2023]. See the Terms and Conditions (https://onlinelibrary.wiley.com/terms-and-conditions) on Wiley Online Library for rules of use; OA articles are governed by the applicable Creative Commons License

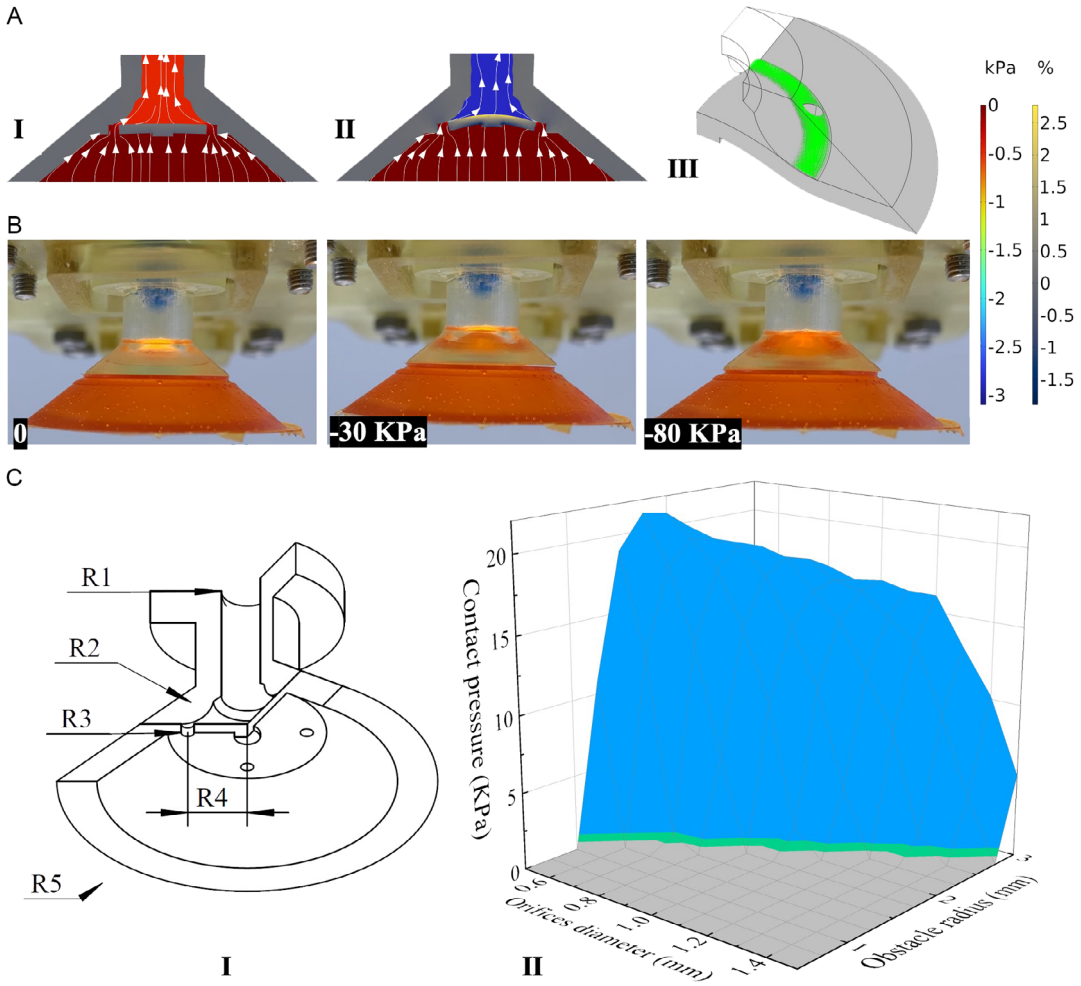

Figure 7. Self-closing principle analysis and validation. A) Fluid–structural interaction simulations. I) The initial fluid field at vacuum −0.8 kPa and SC geometry, the film deformation, and the fluid field at vacuum −3 kPa; strain of the film deformation is indicated by the gray; II) air pressure is indicated by the rainbow, fully closed self-closing structure and contact force area; and III) the maximum contact pressure is 18 kPa. B) Film deformation was observed through the 3D-printed transparent neck at vacuum 0, −30, −80 kPa separately. C) The geometrical dimensions of the self-closing structure. I) R1 = 2 mm, R2 = 2.6 mm, R3 = 0.5 mm, R4 = 4.6 mm, and R5 = 14.7 mm, orifices radius R3 and obstacle radius R2 are the critical dimensions of the self-closing function; II) the contact pressure between the film and ring structure influenced by orifices diameter and obstacle radius.

smaller radius would hinder casting during manufacturing. The radius of the ring structure was varied from 0 to 3 mm. The airtightness of the self-closing mechanism is determined by the contact pressure between the film and the neck. The influence of R2 and R3 on the contact pressure is depicted in Figure 7C (II). Combinations within the gray zone indicate a lack of self-closing. To optimize the contact pressure, a hole radius of 0.5 mm (R3) and a ring structure diameter of 1.8 mm (R2) were chosen. The configuration, with R1 = 2 mm, R2 = 1.8 mm, R3 = 0.5 mm, R4 = 4.6 mm, and R5 = 14.7 mm, resulted in a maximum contact pressure of 23 kPa.

The results of the fluid-structure interaction simulation in the SC are illustrated in Figure 7A. When the vacuum pressure is set to −0.8 kPa, there is airflow through the film's holes, resulting in a pressure difference between the two sides of the film (Figure 7A I). As the vacuum pressure decreases to −3 kPa, the airflow increases, causing the pressure difference to grow and leading to the film's deformation toward the neck (Figure 7A II). At this pressure, the system is not completely sealed, and a small airflow of 0.02 L s^{-1} remains. However, when the vacuum pressure decreases to −80 kPa or lower, the system is fully sealed.

2.4.3. Experimental Validation

For visualizing the self-closing principle, a transparent 3D-printed MSC was created, replacing the DPBM-FT3000-r1 material with Liqcreate Clear Impact resin printed on a Prusa SL1S printer (Figure 7B). The images clearly demonstrate the deformation of the film as the pressure decreases from 0 kPa to −30 kPa and eventually −80 kPa. These deformations align with the simulation results, confirming that a stronger vacuum leads to a greater pressure gradient and ultimately seals off the airflow.

The self-closing MSC was fabricated using a multi-stage casting process. To experimentally test and validate the self-closing

© 2023 The Authors. Advanced Intelligent Systems published by Wiley-VCH GmbH

26404567, 2023, 10, Downloaded from https://onlinelibrary.wiley.com/doi/10.1002/aisy.202300135 by EVIDENCE AID - BELGIUM, Wiley Online Library on [23/11/2023]. See the Terms and Conditions (https://onlinelibrary.wiley.com/terms-and-conditions) on Wiley Online Library for rules of use; OA articles are governed by the applicable Creative Commons License

function, a dedicated characterization setup was developed, consisting of a vacuum generator, a vacuum regulator, and an airflow sensor (**Figure 8**C). A comparison was made between the self-closing MSC and an MSC without the film. The airflow was measured as a function of applied vacuum pressure when the SCs were not in contact (Figure 8A). The self-closing function is only triggered when the air pressure drops below −30 kPa, resulting in zero airflow. This leads to reduced energy consumption in SC array configurations. In contrast, the MSC without self-closing exhibits increasing airflow with higher vacuum levels, reaching a maximum of 19 L min^{-1} limited by the tube size of the connector. In array configurations, this airflow loss translates to higher energy consumption. The airflow serves as a crucial indicator of the energy-saving potential, considering factors like vacuum generators and compressors. To demonstrate the energy-saving function of self-closing SCs, an example is provided. An Airpress Compressor L6-165 Silent (Rated input 0.52 kW, Displacement 25 L min^{-1}) is connected to an SMC Vacuum Ejector ZH05S. When one SC is not in use (without an object attached), the power consumption of the compressor is reduced from 0.25 kW (regular suction) to 0.1 kW (self-closing SC). Figure 8B illustrates the vacuum remaining when SCs are separated from objects. The self-closing MSC maintains the system vacuum at the sealed state, thereby enhancing the performance of soft vacuum grippers with arrays of SCs. In contrast, the MSC without self-closing results in significant vacuum losses when releasing an object.

2.5. Recycling and Reprocessing of the MSC

The reversible DA crosslinks present in both DPBM-FT3000-r1 and DPBM-FT5000-r0.5 elastomers allow for thermal reprocessing above their gel transition temperature using formative manufacturing methods such as casting, compression molding, and injection molding,[51] as well as additive manufacturing techniques.[52] This is in high contrast to traditional elastomers used in industries like NBR (Nitrile butadiene rubber), NR (Natural rubber), and SIR (Silicone), which undergo irreversible crosslinking during manufacturing and cannot be reprocessed. Even when materials can be reprocessed, recycling multi-material components poses significant challenges as disassembling and separating parts is often difficult or even impossible, especially for components that are glued together. In the case of the MSC, however, the two reversible elastomers can be mechanically separated (**Figure 9**) by cutting along the multi-material interface using a scalpel blade. Despite their strong interactions, the DA bond remains the weakest covalent bond in the system, allowing for selective mechanical separation of the materials. This process is facilitated by the absence of external adhesives in the formation of the multi-material component. The separated DPBM-FT5000-r0.5 and DPBM-FT3000-r1 can be individually reprocessed by heating each material above its respective degelation temperature: 92 °C for DPBM-FT5000-r0.5 and 128 °C for DPBM-FT3000-r1. At these transition temperatures, the equilibrium of the DA reaction shifts completely to the unbound state. The reduction in DA crosslinks leads to the loss of the network structure and its associated stability, transforming the polymer from a solid into a liquid structure (Figure 2). This process is fully reversible, as cooling allows the reforming of the DA bonds and the polymer regels into a network structure, ultimately recovering its initial properties. Consequently, heating the separated DPBM-FT5000-r0.5 and DPBM-FT3000-r1 parts to 120 and 140 °C, respectively, causes them to lose their structural stability and flow into a sheet structure (Figure 9). Both sheets can then be reprocessed into the MSC using casting, resulting in a fully recycled SC.

3. Discussion and Conclusions

SCs play a vital role in industrial pick-and-place applications due to their compact design and high adhesive force, making them indispensable in warehouses and assembly lines for their cost-effectiveness and effectiveness. Their compactness also enables their use in array configurations, creating grippers capable of handling objects of various shapes and sizes, aligning with the requirements of versatile warehouse applications. As the manufacturing industry shifts toward mass customization in Industry 4.0, the demand for these flexible manipulator

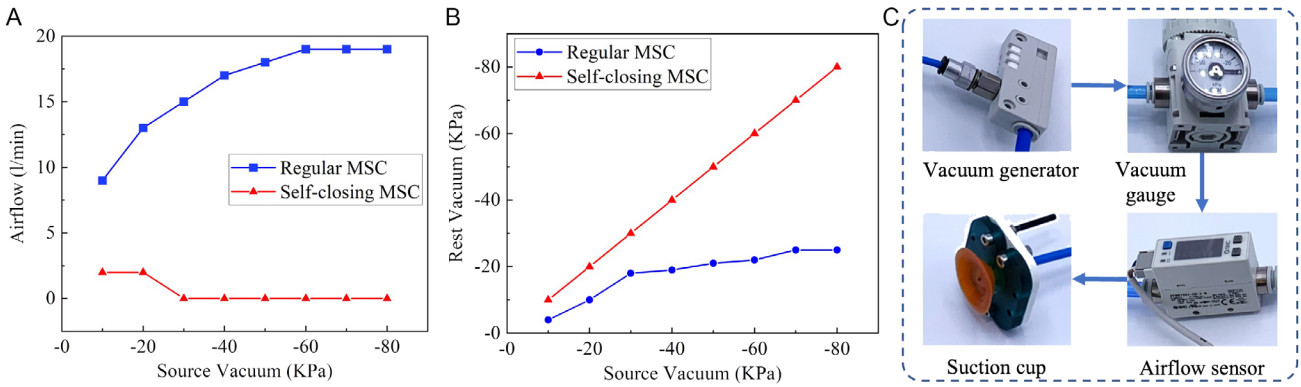

Figure 8. Self-closing and vacuum-saving performance of MSC compared to SCs without self-closing function. A) Leakage when SCs are separated from objects; the self-closing MSC stops leakage from −30 kPa, while regular MSC consistently leaks. B) Rest vacuum when SCs are separated from objects, the vacuum is kept by self-closing MSC while the leakage from regular SCs reduces the vacuum. C) The measurement of SCs vacuum and airflow, a vacuum generator was used to produce desired vacuum up to −80 kPa, a vacuum gauge was used to measure the vacuum, and an airflow sensor was used to measure the airflow.

© 2023 The Authors. Advanced Intelligent Systems published by Wiley-VCH GmbH

26404567, 2023, 10, Downloaded from https://onlinelibrary.wiley.com/doi/10.1002/aisy.202300135 by EVIDENCE AID - BELGIUM, Wiley Online Library on [23/11/2023]. See the Terms and Conditions (https://onlinelibrary.wiley.com/terms-and-conditions) on Wiley Online Library for rules of use; OA articles are governed by the applicable Creative Commons License

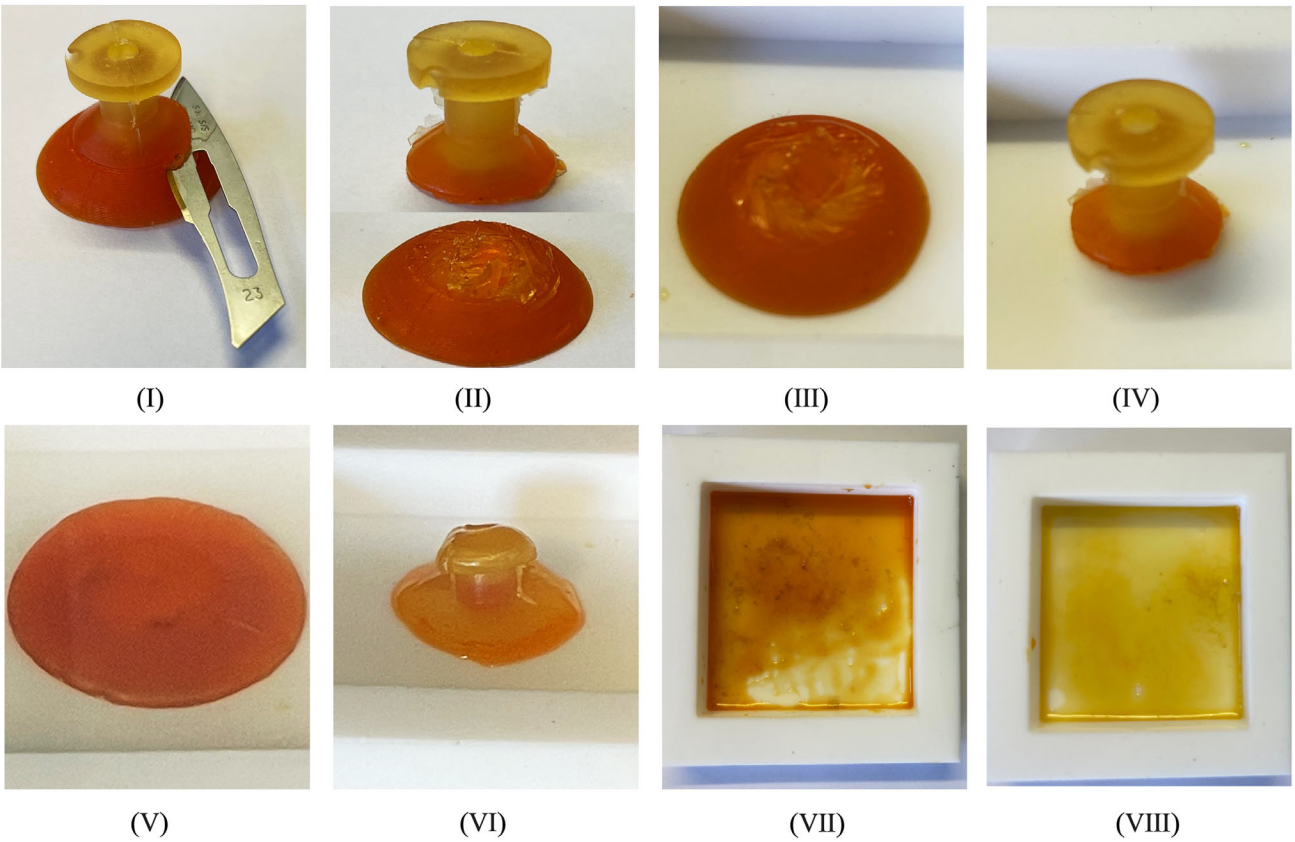

Figure 9. Reprocessing of the MSC via thermal heating. I and II) First, the multi-material part is separated to by cutting. III and IV) Then, they are put in the oven and separately heated up to 120 and 140 °C. V and VI) DPBM-FT5000-r0.5 and DPBM-FT3000-r1 gradually lose stiffness and degel. VII and VIII) In the end, these two parts of the SC complete degelation.

platforms is expected to grow further. Despite their widespread adoption, SC-based systems encounter energy losses that have been addressed in this paper. These losses stem from inadequate contact, damaged SCs, and unconnected SCs within the array. When significant, these air losses diminish the system's performance by reducing the vacuum pressure and subsequently the adhesive force. In contrast to previous solutions, our paper presented a holistic approach to these three issues by introducing a versatile (i), self-healing (ii), and self-closing (iii) MSC. The incorporation of these new capabilities maintains the compactness of the cups without increasing their dimensions, distinguishing it from many state-of-the-art solutions. To achieve versatility, self-healing, and recyclability (iv), reversible elastomers containing reversible crosslinks formed by a DA reaction were utilized.

3.1. Versatility

The presented MSC is versatile as it can grasp and move small and large objects with different shapes, sizes, and roughness by combining a hyper-flexible and a stiff reversible elastomer. This is achieved by combining a hyper-flexible bottom part and a stiff reversible elastomer. The hyper-flexible bottom ensures optimal contact with irregular or angled surfaces, even with low vacuum power. The MSC can effectively seal rough surfaces by applying minimal force, making it suitable for handling delicate items such as fruits and vegetables in agrifood applications without causing damage. The stiff elastomer used for the neck of the MSC provides robustness and stability during pick and place operations, which is crucial for high-speed applications. Both the hyper-flexible and stiff parts contain the same DA crosslinks in their polymer network, allowing them to be chemically bonded through a heat–cool cycle. Tensile testing confirmed the high strength of the resulting multi-material interface, distinguishing it from MSCs or soft robotic components in the literature that rely on adhesion and are prone to delamination and failure over time. This problem of weak multi-material interfaces is a primary reason why SCs in industries are typically made from a single material. The use of reversible elastomers addresses this issue and enables the creation of robust MSCs that combine versatility with stability.

3.2. Self-Healing

Increasing the flexibility of SCs enhances their versatility, but it also introduces a vulnerability to damage from sharp objects in the environment. This challenge was addressed by manufacturing SCs like the MSC using reversible DA elastomers, which possess inherent self-healing capabilities. The healing process

© 2023 The Authors. Advanced Intelligent Systems published by Wiley-VCH GmbH

26404567, 2023, 10, Downloaded from https://onlinelibrary.wiley.com/doi/10.1002/aisy.202300135 by EVIDENCE AID - BELGIUM, Wiley Online Library on [23/11/2023]. See the Terms and Conditions (https://onlinelibrary.wiley.com/terms-and-conditions) on Wiley Online Library for rules of use; OA articles are governed by the applicable Creative Commons License

requires molecular mobility, which is present at room temperature in the softest DA material used for the bottom part of the MSC. As a result, damages such as punctures, tears, and cuts in the soft part can completely heal within 24 h, restoring the full performance as demonstrated by material-level tensile testing. However, in applications where a 24 h downtime is unacceptable, the healing time can be significantly reduced by increasing the temperature to 80 °C, enabling full recovery in just one hour. The choice between a simpler design with a healing time of a day or faster healing with a more complex system incorporating an integrated heater depends on the specific application and the desired trade-off. Although the stiff neck of the MSC is less exposed to sharp objects, it also has the ability to heal. However, at room temperature, the stiff elastomer exhibits limited molecular mobility and cannot heal autonomously. Nonetheless, raising the temperature to 90 °C for one hour provides sufficient mobility to facilitate healing in this part of the MSC as well. Incorporating a healing capacity in SCs can offer economic benefits, particularly for systems operating remotely or in complex environments where maintenance is challenging. Extending the lifespan of SCs contributes to sustainability by reducing plastic consumption.

3.3. Self-Closing

This paper introduced a novel geometrical design that imparts self-closing functionality to a SC when it is not in contact with the grasping object. The self-closing mechanism relies on a flexible film featuring four holes that are sealed when the film deforms due to the pressure difference that is generated by the airflow during suction without contact. Through fluid-structural interaction simulations utilizing FEA, the design was optimized to achieve self-closure at pressures below −30 kPa. While this principle was integrated into the MSC, it can be adapted to almost any SC. The sensitivity of the self-closing system, characterized by the minimal pressure difference required to activate it, can be adjusted for specific applications using various design parameters detailed in the paper. The presented FEA framework offers a means to fine-tune the design of self-closing SCs based on specific application requirements. When employed in an array configuration, such self-closing cups can result in significant energy savings. This passive system operates without the need for control, exemplifying embodied intelligence. Furthermore, the self-closing mechanism is seamlessly integrated into the SC without increasing its size, enabling direct application to existing SC array systems without modifications.

3.4. Recycling

Lastly, a new method for recycling multi-material elastomeric components was showcased through the reprocessing of the MSC. Unlike the currently employed elastomers in widely used SCs, such as silicones and rubbers, which are non-reprocessable, the DA elastomers in the MSC possess reversible crosslinks that enable thermal reprocessing. By heating them above their gel transition temperature, typically around 120°–140°, the elastomers can undergo recycling. For multi-material DA parts like the MSC, two recycling approaches exist. In the first approach, the entire multi-material part is degelled into a liquid state by heating it above the degelation temperature of both DA elastomers. The resulting liquid materials can be mixed and cast to produce reversible elastomers with intermediate mechanical properties. Although these recycled elastomers cannot be used to recreate an MSC, they can find applications in other contexts. In the second approach outlined in this paper, the materials are separated before reprocessing. By mechanically separating the parts, such as through cutting, only the reversible DA bonds are broken. Consequently, the two separated parts can be individually degelled by heating them above their respective degelation temperatures and subsequently reprocessed. An additional advantage of the employed DA elastomers is that their reprocessing can be conducted under mild conditions, typically between 120–140 °C.

The authors believe that the integration of versatility, robustness, self-healing, self-closing, and recyclability, as proposed in this paper, is crucial for the development of environmentally friendly vacuum grippers that contribute to a sustainable future. The utilization of FEA-based fluid-structural interaction simulations has significantly reduced the cost associated with developing fluidic-driven soft devices, enabling researchers to analyze physical variables more effectively. Moreover, the computational capabilities of FEA facilitate the seamless integration of novel designs into diverse applications with varying materials and dimensions.

4. Experimental Section

FEA: The 3D structural geometry of the self-closing MSC and the inner fluid domain were built in SolidWorks by the parametric modeling method. The geometry was synced into COMSOL Multiphysics to compute FEA simulations. The two DA elastomers, the DPBM-FT5000-r0.5 and the DPBM-FT3000-r1, were simulated as linear elastic materials with Young's moduli of 0.12 and 54 MPa. Because of the material strain within a small scale, the hyper-elasticity of the self-healing materials affected little on the results. The FEA simulation work focused on the exploitation and analysis of the self-closing mechanism and the parameterized structural optimization. The fluid–structural interaction model was used for self-closing mechanism exploitation and analysis. The mesh for fluid–structural interaction simulation contained 180 274 elements. A time-dependent solver with a time-steeping method backward differentiation formula was employed to solve the physics model. The parametric sweep function was employed to analyze the critical geometrical size.

Monomers: The triamine Jeffamines T3000 and T5000 had trifunctional polypropylene glycol backbones and average molar masses of 3240 and 5709 g mol^{-1}, respectively. The Jeffamines were supplied by Huntsman (Belgium). Furfuryl glycidyl ether (FGE), with a purity of 95%, was purchased from Sage Chemicals (China) and stored in refrigerated conditions. 1,1-(Methylenedi-4,1-phenylene)-bismaleimide (DPBM), with a purity of 95% and a molar mass per functionality (M_M) of 189 g mol^{-1}, was obtained from Sage Chemicals (China). 4-tert-butylcatechol was used as a radical inhibitor and was supplied by Sigma–Aldrich. All chemicals were used as delivered.

Synthesis: The reversible elastomers, DPBM-FT3000-r1 and DPBM-FT5000-r0.5, were synthesized in a two-step, solventless synthesis. First, FGE was reacted with a stoichiometric amount of Jeffamine, yielding a furan-functionalized Jeffamine FT3000 or FT5000 compound with a molar per functionality (M_F) of 691 or 1112 g mol^{-1}. The irreversible reaction was performed for a minimum of 7 days at 60 °C under continuous magnetic stirring, after which the reaction was completed for 2 days at 90 °C. For the next step, first the DPBM crystals (melting temperature was 155 °C) and 4-tert-butylcatechol crystals (5 wt% of DPBM, melting temperature at 50 °C) were melted at 160 °C, increasing their solubility.

© 2023 The Authors. Advanced Intelligent Systems published by Wiley-VCH GmbH

26404567, 2023, 10, Downloaded from https://onlinelibrary.wiley.com/doi/10.1002/aisy.202300135 by EVIDENCE AID - BELGIUM, Wiley Online Library on [23/11/2023]. See the Terms and Conditions (https://onlinelibrary.wiley.com/terms-and-conditions) on Wiley Online Library for rules of use; OA articles are governed by the applicable Creative Commons License

Next, hot FT3000 or FT5000 (at 160 °C) was added with a stoichiometric maleimide to furan ratio of 1 or 0.5 ($r = [M_0]/[F_0]$, with $[M_0]$ and $[F_0]$ the maleimide and furan concentrations). To synthesize material with a total mass of m_t, following masses of FT3000 or FT5000 (m_F) and DPBM (m_M) were needed

$$m_M = \frac{m_t}{\frac{1}{r}\frac{M_F}{M_M} + 1} \quad , \quad m_F = \frac{m_t}{r\frac{M_M}{M_F} + 1} \tag{1}$$

where r is the stoichiometric maleimide-to-furan ratio (unitless) and M_M and M_F are the average molar masses per functionality of DPBM and FT3000 or FT5000, respectively (g mol^{-1}). Immediately after pouring the hot FT3000 or FT5000 on the DPBM melt, the parts were mixed for 1 min using a magnetic stirrer. Bubbles that were induced by mixing were removed by inserting the mixture in an Eppendorf centrifuge 5804 at 5000 rpm for 2 min. Afterward, the degassed mixture was cast in an appropriate mold. The mixture reacted into a DPBM-FT5000-r0.5 or DPBM-FT3000-r1 elastomer due to DA cross-linking. After 24 h at ambient conditions, the polymer network was completely formed, and stable material properties were reached. By changing the Jeffamine monomer and/or the stoichiometric ratio r, the mechanical properties of the reversible elastomers could be tuned over a broad range from hyperelastic (100 kPa range) to very stiff (GPa range).[48]

Fabrication of SCsAll: SCs were cast in molds, that were 3D printed using an SLA 3D printing (PRUSA SL1 Speed) with resin (3DJAKE Color Mix Resin Basic). The 3D models of SCs and molds were designed in SolidWorks. In the last step of the synthesis, the DPBM-FTxxx-rx material was cast inside the mold. Upon cooling down, the elastomeric network was formed through the DA reaction that acted as a cross-linker. The single-material SSC and HSC were cast in a single molding procedure. The MSC in contrast was created by first molding the stiff top part (DPBM-FT3000-r1) and the bottom hyper-flexible part (DPBM-FT5000-r0.5) separately. Next, the molded parts were chemically bonded through a heat–cool cycle at 90 °C (Figure 8A). During this last step, both parts remained solid and there was no need for a mold.

SC Characterization: The dedicated test bench for the characterization of the SCs consisted of a compressed air source (Airpress Compressor L 6-165 Silent), a vacuum generator (SMC ZH10B), a flowmeter (SMC PFM7 Series Flow Switch), and a vacuum regulator (SMC vacuum regulator series IRV10) (Figure 8C). This setup allowed us to quantitatively measure the vacuum and airflow consumed by SCs. To measure the maximum adhesion force, the SCs were mounted on a tensile machine (Tinius Olsen 5ST). The connectors were designed in SolidWorks and 3D printed using filaments in Prusa i3. Next, the SCs were mounted on a robotic manipulator (Rotrics DexArm).

Supporting Information

Supporting Information is available from the Wiley Online Library or from the author.

Acknowledgements

This research is funded by the EU Project SHINTO (grant no. 101057960) and ITN project SMART (grant no. 860108). Zhanwei Wang is funded by China Scholarship Council (CSC). The FWO (Fonds Wetenschappelijk Onderzoek) funded the work through personal grants of Seppe Terryn (grant no. 1100416N), Julie Legrand (grant no. 12Y8622N), and Joost Brancart (grant no. 12E1123N). H.W. is funded by ITN project SMART (grant no. 860108).

Conflict of Interest

The authors declare no conflict of interest.

Data Availability Statement

The data that support the findings of this study are available from the corresponding author upon reasonable request.

Keywords

energy-saving, self-closing, self-healing, soft robotics, vacuum gripper

Received: March 16, 2023
Revised: July 14, 2023
Published online: August 21, 2023

[1] S. Nansai, R. Mohan, *Robotics* **2016**, *5*, 14.
[2] Z. Xie, A. G. Domel, N. An, C. Green, Z. Gong, T. Wang, E. M. Knubben, J. C. Weaver, K. Bertoldi, L. Wen, *Soft Rob.* **2020**, *7*, 639.
[3] M. A. Robertson, J. Paik, *Sci. Rob.* **2017**, *2*, eaan6357.
[4] H. Jiang, E. W. Hawkes, C. Fuller, M. A. Estrada, S. A. Suresh, N. Abcouwer, A. K. Han, S. Wang, C. J. Ploch, A. Parness, M. R. Cutkosky, *Sci. Rob.* **2017**, *2*, eaan4545.
[5] H. Lee, D.-S. Um, Y. Lee, S. Lim, H.-J. Kim, H. Ko, *Adv. Mater.* **2016**, *28*, 7457.
[6] Y. Wang, G. Sun, Y. He, K. Zhou, L. Zhu, *Bioinspiration Biomimetics* **2022**, *17*, 036005.
[7] G. Mantriota, A. Messina, *Mech. Mach. Theory* **2011**, *46*, 607.
[8] T. Lien, in *Robotics and Automation in the Food Industry*, Elsevier, Amsterdam **2013**, pp. 143–170.
[9] A. K. Jaiswal, B. Kumar, *Int. J. Innovative Sci.* **2017**, *4*, 8.
[10] Z. Long, Q. Jiang, T. Shuai, F. Wen, C. Liang, *IOP Conf. Series: Mater. Sci. Eng.* **2020**, *782*, 042055.
[11] H. Kuolt, T. Kampowski, S. Poppinga, T. Speck, R. Tautenhahn, A. Moosavi, J. Weber, F. Gabriel, E. Pierri, K. Dröder, in *Technologies for Economic and Functional Lightweight Design* (Eds.: K. Dröder, T. Vietor), Springer, Berlin, Heidelberg, **2021**, pp. 182–188.
[12] R. Schaffrath, E. Jäger, G. Winkler, J. Doant, M. Todtermuschke, *Procedia CIRP* **2021**, *97*, 76.
[13] T. Matsuno, A. Kakogawa, S. Ma, in *2013 IEEE Int. Conf. on Robotics and Automation*, IEEE, Karlsruhe, Germany, **2013**, pp. 1362–1367.
[14] E. Papadakis, F. Raptopoulos, M. Koskinopoulou, M. Maniadakis, In *2020 6th Int. Conf. on Mechatronics and Robotics Engineering (ICMRE)*, IEEE, Barcelona, Spain, **2020**, pp. 73–77.
[15] P. Motzki, J. Kunze, B. Holz, A. York, S. Seelecke, in (Ed.: W.-H. Liao), *SPIE Smart Structures and Materials + Nondestructive Evaluation and Health Monitoring (SS/NDE)*, San Diego, CA, **2015**, p. 943116.
[16] F. Welsch, S.-M. Kirsch, P. Motzki, M. Schmidt, S. Seelecke, in *SMASIS 2018: Proc. of the ASME 2018 Conf. on Smart Materials, Adaptive Structures and Intelligent Systems*, Volume 1, American Society of Mechanical Engineers, San Antonio, TX, **2018**, p. V001T04A014.
[17] C. Daut, S.-M. Kirsch, F. Welsch, S. Seelecke, P. Motzki, in *SMASIS 2021: Proc. of the ASME 2021 Conf. on Smart Materials, Adaptive Structures and Intelligent Systems*, American Society of Mechanical Engineers, Virtual Conference, **2021**, p. V001T03A003.
[18] P. Lyu, M. O. Astam, C. Sánchez-Somolinos, D. Liu, *Adv. Intell. Syst.* **2022**, *4*, 2200280.
[19] P. Zhang, M. Kamezaki, K. Otsuki, Z. He, H. Sakamoto, S. Sugano, in *2020 IEEE/ASME Inter. Conf. on Advanced Intelligent Mechatronics (AIM)*, IEEE, Boston, MA, **2020**, pp. 777–782.
[20] H. Kuolt, T. Kampowski, S. Poppinga, T. Speck, A. Moosavi, R. Tautenhahn, J. Weber, F. Gabriel, E. Pierri, K. Dröder, in *12th International Fluid Power Conf.*, Technische Universität, Dresden, **2020**, Vol. 3, pp. 17–26.

© 2023 The Authors. Advanced Intelligent Systems published by Wiley-VCH GmbH

26404567, 2023, 10, Downloaded from https://onlinelibrary.wiley.com/doi/10.1002/aisy.202300135 by EVIDENCE AID - BELGIUM, Wiley Online Library on [23/11/2023]. See the Terms and Conditions (https://onlinelibrary.wiley.com/terms-and-conditions) on Wiley Online Library for rules of use; OA articles are governed by the applicable Creative Commons License

[21] J. Liu, K. Tanaka, L. Bao, I. Yamaura, *Vacuum* **2006**, *80*, 593.
[22] G. Mantriota, *Mech. Mach. Theory* **2007**, *42*, 18.
[23] J. Mahler, M. Matl, X. Liu, A. Li, D. Gealy, K. Goldberg, in *2018 IEEE Int. Conf. on Robotics and Automation (ICRA)*, IEEE, Brisbane, QLD, **2018**, pp. 5620–5627.
[24] F. Gabriel, S. Baars, M. Römer, K. Dröder, *Machines* **2021**, *9*, 149.
[25] H. Zhang, J. Peeters, E. Demeester, K. Kellens, *J. Intell. Rob. Syst.* **2021**, *103*, 64.
[26] M. Maggi, G. Mantriota, G. Reina, *Actuators* **2022**, *11*, 55.
[27] T. M. Huh, K. Sanders, M. Danielczuk, M. Li, Y. Chen, K. Goldberg, H. S. Stuart, in *2021 IEEE/RSJ Inter. Conf. on Intelligent Robots and Systems (IROS)*, IEEE, Prague, Czech Republic, **2021**, pp. 1786–1793.
[28] H. Tsukagoshi, Y. Osada, *Actuators* **2021**, *10*, 50.
[29] T. Takahashi, M. Suzuki, S. Aoyagi, in *2016 IEEE 11th Annual Inter. Conf. on Nano/Micro Engineered and Molecular Systems (NEMS)*, IEEE, Sendai, Japan, **2016**, pp. 508–511.
[30] Z. Zhakypov, F. Heremans, A. Billard, J. Paik, *IEEE Rob. Autom. Lett.* **2018**, *3*, 2894.
[31] H. J. Lee, S. Baik, G. W. Hwang, J. H. Song, D. W. Kim, B.-Y. Park, H. Min, J. K. Kim, J.-S. Koh, T.-H. Yang, C. Pang, *ACS Nano* **2021**, *15*, 14137.
[32] S. Jeong, P. Tran, J. P. Desai, *IEEE Rob. Autom. Lett.* **2020**, *5*, 867.
[33] C. C. Kessens, J. P. Desai, *J. Mech. Rob.* **2011**, *3*, 045001.
[34] T. Yue, W. Si, A. J. Partridge, C. Yang, A. T. Conn, H. Bloomfield-Gadelha, J. Rossiter, *IEEE Rob. Autom. Lett.* **2022**, *7*, 3600.
[35] M. Li, A. Pal, A. Aghakhani, A. Pena-Francesch, M. Sitti, *Nat. Rev. Mater.* **2021**, *7*, 235.
[36] P. Rothemund, A. Ainla, L. Belding, D. J. Preston, S. Kurihara, Z. Suo, G. M. Whitesides, *Sci. Rob.* **2018**, *3*, eaar7986.
[37] M. Cianchetti, A. Arienti, M. Follador, B. Mazzolai, P. Dario, C. Laschi, *Mater. Sci. Eng. C* **2011**, *31*, 1230.
[38] A. Koivikko, D.-M. Drotlef, C. B. Dayan, V. Sariola, M. Sitti, *Adv. Intell. Syst.* **2021**, *3*, 2100034.
[39] S. Song, D.-M. Drotlef, D. Son, A. Koivikko, M. Sitti, *Adv. Sci.* **2021**, *8*, 2100641.
[40] T. Tomokazu, S. Kikuchi, M. Suzuki, S. Aoyagi, in *2015 IEEE/RSJ Inter. Conf. on Intelligent Robots and Systems (IROS)*, IEEE, Hamburg, **2015**, pp. 2929–2936.
[41] S. T. Frey, A. B. M. T. Haque, R. Tutika, E. V. Krotz, C. Lee, C. B. Haverkamp, E. J. Markvicka, M. D. Bartlett, *Sci. Adv.* **2022**, *8*, eabq1905.
[42] M. Sitti, *Extreme Mech. Lett.* **2021**, *46*, 101340.
[43] F. Tramacere, A. Kovalev, T. Kleinteich, S. N. Gorb, B. Mazzolai, *J. R. Soc. Interface* **2014**, *11*, 20130816.
[44] S. M. Fossati, F. Carella, G. De Vico, F. Benfenati, L. Zullo, *J. Exp. Mar. Biol. Ecol.* **2013**, *447*, 93.
[45] A. Tiwari, B. N. J. Persson, arXiv:1905.09042 [cond-mat], **2020**.
[46] E. Roels, S. Terryn, J. Brancart, G. Van Assche, B. Vanderborght, in *2019 2nd IEEE Int. Conf. on Soft Robotics (RoboSoft)*, IEEE, Seoul, **2019**, pp. 316–321.
[47] S. Terryn, E. Roels, J. Brancart, G. Van Assche, B. Vanderborght, *Actuators* **2020**, *9*, 34.
[48] S. Terryn, J. Brancart, E. Roels, R. Verhelle, A. Safaei, A. Cuvellier, B. Vanderborght, G. Van Assche, *Macromolecules* **2022**, *55*, 5497.
[49] A. Safaei, S. Terryn, B. Vanderborght, G. Van Assche, J. Brancart, *Polymers* **2021**, *13*, 2522.
[50] S. K. Tabrizian, F. Sahraeeazartamar, J. Brancart, E. Roels, P. Ferrentino, J. Legrand, G. Van Assche, B. Vanderborght, S. Terryn, *IEEE Rob. Autom. Lett.* **2022**, *7*, 4574.
[51] Z. Wang, S. Terryn, J. Legrand, P. Ferrentino, S. K. Tabrizian, J. Brancart, E. Roels, G. Van Assche, B. Vanderborght, in *2022 IEEE/RSJ Int. Conf. on Intelligent Robots and Systems (IROS)*, IEEE, Piscataway, NJ **2022**, pp. 5448–5455.
[52] E. Roels, S. Terryn, J. Brancart, R. Verhelle, G. Van Assche, B. Vanderborght, *Soft Rob.* **2020**, *7*, 711.

© 2023 The Authors. Advanced Intelligent Systems published by Wiley-VCH GmbH

26404567, 2023, 10, Downloaded from https://onlinelibrary.wiley.com/doi/10.1002/aisy.202300135 by EVIDENCE AID - BELGIUM, Wiley Online Library on [23/11/2023]. See the Terms and Conditions (https://onlinelibrary.wiley.com/terms-and-conditions) on Wiley Online Library for rules of use; OA articles are governed by the applicable Creative Commons License